In Situ Surface-Enhanced Infrared Spectroscopy to Identify Oxygen Reduction Products in Non-aqueous Metal-Oxygen Batteries

J. Padmanabhan Vivek†, Neil G. Berry†, Jianli Zou†, Richard J. Nichols† and Laurence J. Hardwick*†

†Stephenson Institute for Renewable Energy, Department of Chemistry, University of Liverpool, Liverpool L69 7ZD, United Kingdom.

ABSTRACT

We report on the detection of metastable, solvated and surface adsorbed alkali metal-oxygen (M-O_2) discharge species using *in situ* attenuated total reflectance surface enhanced infrared absorption spectroscopy (ATR-SEIRAS). Oxygen-oxygen stretching bands (ν_{O-O}) of superoxide species formed during M-O_2 battery discharge have been challenging to observe by conventional infrared (IR) techniques and because of this, there has been limited use of IR techniques for *in situ* monitoring of the discharge products at the cathode in metal-O_2 batteries. We explore SEIRAS technique to investigate lithium-oxygen and sodium-oxygen electrochemistry in acetonitrile (MeCN; a low Gutmann donor number solvent) as well as dimethyl sulfoxide (DMSO; a high Gutmann donor number solvent) in order to demonstrate the feasibility of our approach in the ongoing efforts toward the realization of M-O_2 battery technology. *In situ* IR spectroscopy studies, together with coupled-cluster method including perturbative triple excitations [CCSD (T)] calculations, establishes that certain M-O and O-O stretching bands (ν_{M-O} and ν_{O-O}) of metal superoxide and peroxide molecular species are IR active, although these vibrational modes are silent or suppressed in their crystalline forms. An *in situ* IR spectroscopy based approach to distinguish between 'solution mediated' and 'surface confined' discharge pathways in non-aqueous M-O_2 batteries is demonstrated.

Introduction

Lithium-ion batteries have revolutionized technological progress of the past two decades; however, there appears to be little room left to increase further their specific energy[1]. Developing new types of batteries with higher energy storage and superior performance is crucial for the realisation of a true alternative to fossil-fuel-based energy economy[1, 2]. In view of the overwhelmingly high gravimetric energy densities projected by theoretical as well as recent experimental reports, metal-oxygen (M-O_2) batteries, popularly known as metal-air batteries, promise to lead next generation energy storage systems.[1-16] While the cathodes of metal-ion batteries rely on the intercalation reactions of metal ions, non-aqueous M-O_2 batteries are based on the electrochemical reduction of molecular oxygen and their subsequent reaction with metal ions at the cathode. Under controlled conditions, the M-O_2 electrochemical reaction products can be reversibly oxidised to regenerate molecular oxygen (O_2) at the cathode and the corresponding metal (M = Li or Na) at the anode, making it a promising secondary battery. In spite of its huge advantage in terms of specific energy, currently several detrimental physical and chemical mechanisms during the charge-discharge process prevents M-O_2 becoming a practical technology.[1-3, 17-20] Therefore, fundamental studies providing molecular level understanding and mechanistic insight into the underlying interfacial electrode processes during discharge-charge (electro) chemistry, as wells as other desirable or undesirable reaction pathways are required in order for M-O_2 batteries to develop into a technology of the near future[2].

There has been tremendous effort in the area of non-aqueous Li-O_2 batteries in the past few years that have given some significant insights, yet several unresolved issues prevent the realization of a sustainable Li-O_2 battery. Recently, several groups have shifted attention to other M-O_2 batteries as well, particularly Na-O_2, with the aim of surpassing certain limitations and challenges in the Li-

O_2 system. Na-O_2 batteries have been proposed as a more reversible, stable and energy efficient system in a series of recent reports,[15, 16, 21] however Na-O_2 research is still in its infancy and there is a need to address several issues in this area as well. More importantly, the storage capacity, reversibility as well as discharge products of M-O_2 batteries depend on the electrolyte composition as well.[22-25] The complexity and sensitivity of the discharge/charge reactions recognized by recent reports underlines the importance of detailed, theoretical as well as experimental, mechanistic investigations under controlled conditions in order to fill in the knowledge-gap hampering M-O_2 battery technology.

The improvements and insights obtained in the area of M-O_2 batteries in recent years hugely benefited from in-depth *in situ* analyses. Notably, *in situ* Raman spectroelectrochemistry has played a key role in revealing intricate details of charge-discharge chemistry at the electrode/electrolyte interface in these systems.[17, 23, 26-28] There have also been attempts to utilize *in situ* infrared (IR) spectroscopy in this direction, but conventional *in situ* infrared spectroscopy techniques suffer from huge IR absorption by the electrolyte, making interfacial analysis of model battery interfaces a challenging task. A recent study also highlights the limitations of *ex situ* IR spectroscopy techniques in the context of electrode-electrolyte interface characterization in Li-O_2 cell positive electrodes.[29] This study points out that even compounds such as lithium carbonate (carbonates have high IR absorption cross section compared to peroxides or superoxides) need to be present at significant concentrations ($\geq$ 6-8 mol%) in carbon matrices (typical positive electrode for lithium-oxygen batteries) to be able to detect them using *ex situ* IR spectroscopy. Apart from these issues, the deployment of IR techniques with the goal of identifying oxygen reduction products is questionable for the simple reason that typical oxygen reduction reaction (ORR) products such as superoxides and peroxides often do not have IR active $\nu_{O\text{-}O}$. In spite of this, our motivation stems

from the fact that these stretching modes in MO_2 can be IR active under certain conditions where O-O bonds deviate from their innate homopolar nature. IR detection of superoxides and peroxides of lithium and sodium have been reported in matrix isolated systems,[30-33] yet the detection of M_xO_2 species in solution or at the interface remains unreported. The detection of electrochemically generated reduced oxygen species using *in situ* attenuated total reflectance (ATR) IR spectroscopy or surface enhanced infrared absorption spectroscopy (SEIRAS) techniques in alkaline and acidic media has been reported a few times.[34-36] However, there have been no reports exploring SEIRAS techniques for studying oxygen reduction mechanisms in non-aqueous environments, especially in the area of M-O_2 batteries. Our IR based approach was inspired by the recent reports suggesting solution mediated discharge mechanisms in non-aqueous M-O_2 batteries. According to this postulate, the discharge product formation in non-aqueous M-O_2 may follow a solution mediated or surface confined mechanism determined by the donicity of the solvent.[22] In solution-mediated processes, M-O_2 intermediates were formed in the solution rather than on the electrode surface. If these discrete, intermediary ORR species formed in solution can be detected using SEIRAS, this would open up the scope of this approach in areas beyond M-O_2 batteries, viz. catalysis, fuel cells, biomimetic electrochemical systems, etc.

During the discharge of an M-O_2 battery, oxygen is reduced at the cathode, forming nucleophilic oxygen species such as superoxides (O_2^-) and peroxides (O_2^{2-}). Undesirable reactions promoted by these highly nucleophilic species result in the degradation of the electrolytes. Recent efforts toward developing electrolytes that are stable against reactive oxygen species, as well as understanding the mechanistic details of the reaction pathways have led to interesting insights into the Li-O_2 (electro)chemistry. Bruce and co-workers investigated the mechanistic details of the cathode process demonstrating ORR in several aprotic solvent - lithium salt combinations, and their *in situ*

Raman studies explicitly showed the crucial role played by the solvent donicity in determining the discharge chemistry and reversibility of Li-O_2 system.[22] High donor number solvents (e.g. dimethyl sulfoxide [DMSO]) have stronger coordination to the metal cations thereby reducing the Lewis acidity of the cations, thus extending the life of superoxide in solution, where the reaction proceeds *via* chemical disproportionation of superoxides to peroxides. Low donor number solvents (e.g. acetonitrile [MeCN]) promote a surface confined route to lithium superoxide (LiO_2); rather than chemical disproportionation of superoxides to peroxides, a surface growth model of the intermediates and products, is highly likely in this case.[22, 25] Since the report by Johnson *et al.*[15] demonstrated the influence of Gutmann donor number in dictating the solubility, stabilization and growth mechanism of LiO_2 and lithium peroxide (Li_2O_2), there have been tremendous efforts to explore this phenomenon in analogous systems using various *in situ* techniques such as Raman Spectroscopy, Electron Paramagnetic Resonance (EPR), Electrochemical Quartz Crystal Microbalance (EQCM), etc.[26, 37-40] as to identify intermediates and products in Li-O_2 systems. Recently our group has explored the solvent dependence of Na-O_2 electrochemistry using *in situ* Surface Enhanced Raman Spectroscopy (SERS).[26]

In situ SERS has played a crucial role in shedding light on the intricate electrochemistry in M-O_2 cells in the recent years.[22, 23, 26, 28, 41, 42] Various *ex situ* as well as *in situ* IR studies are also being routinely used in this context.[43] We have recently explored the use of ATR-SEIRAS for gaining mechanistic insight into electrolyte degradation pathways.[44] ATR-SEIRAS is a fascinating internal reflection technique that offers superior sensitivity to the interfacial region when compared to other ATR or external reflection techniques. The SEIRA phenomenon (an enhancement in IR absorption in internal reflection IR spectroscopy) was first reported by Hartstein *et al.*[45], followed by the reports by Hatta *et al.*[46] employing an ATR configuration using metal underlayer (Kretschmann

configuration)[47] for signal enhancement. The acronym SEIRAS was first used by Osawa[48] who then pioneered the use of this technique in the area of spectroelectrochemistry.[49-51] SEIRAS has a rich record of accomplishment for studying molecular structure, orientation and functional changes of species present at the electrode/electrolyte interface. A majority of these studies were performed with aqueous electrolytes and used electrolessly deposited metal film on a silicon internal reflection element (IRE). This offers a practical spectroscopic window between 1200 cm^{-1} and 4000 cm^{-1}. IR bands of ORR products of interest generally appear below 1200 cm^{-1}, hence the use of silicon IREs limit the use of SEIRAS for this purpose. We explore the use of ZnSe IRE instead of Si, a major advantage of this being the possibility to study lower wavenumber regions. Since ZnSe is not stable under the conditions in which the gold working electrode film is formed on the IRE by electroless deposition, we have adopted a thermal evaporation technique for this purpose.

Experimental

In situ Electrochemical SEIRAS

A Bruker IFS66v spectrometer equipped with MCT (mercury cadmium telluride; low frequency cut off ca. 550 cm^{-1}) detector was used to record IR spectra (detector range x-y cm-1). The interferometer was driven by dry air; the specular reflection unit was also purged with carbon dioxide free dry air. The angle of incidence was set at 65° and p-polarized IR radiation was used. Electrochemical measurements were performed using a Bio-Logic potentiostat. A schematic of the spectroelectrochemical cell is shown in Figure 1a. A 60° ZnSe prism (PIKE Technologies) was chosen as the ATR internal reflection element. The gold film working electrode (~20 nm thickness) was formed on the polished side of a ZnSe prism, which was thoroughly cleaned in deionized water, sonicated in ethanol then dried overnight prior to gold deposition. The gold film was formed on the ZnSe prism by vacuum deposition of Au (99.999 %) using a Leybold Univex 300 thermal evaporation system. SEM as well as AFM images illustrating the morphology and thickness of the gold island film formed on the prisms are shown in Figure 1. In order to ensure a proper electrical contact to the gold island film, a thicker layer of gold (ca. 40 nm) was deposited around the rim of the gold covered face of ZnSe and electrical contact to the working electrode was made by pressing a gold foil against this. The spectroelectrochemical cell was formed by a PEEK liquid cup attached on top of a ZnSe prism in the Kretschmann configuration. Both counter (Pt) and reference (Ag) electrodes were attached to a PEEK disk and pressed against the top end of the PEEK liquid cup. On both ends of the PEEK liquid cup, a proper seal was ensured using Kalrez® O-rings.

A coiled platinum wire was used as a counter electrode and silver wire as reference electrode. This silver quasi-reference electrode was calibrated against an internal ferrocene reference and potentials were then quoted against either Li/Li^+ or Na/Na^+ for convenient reference. The ATR-SEIRAS cell components and the salts used were dried at 120 °C under vacuum for 12 h and transferred to the glovebox without exposure to air or moisture. The *in situ* SEIRAS cell was assembled and the electrolytes were purged using either dry argon or dry oxygen passed through multiple desiccant columns, inside an argon filled glovebox. Anhydrous Superdry® solvents, MeCN and DMSO were purchased from ROMIL and further dried over activated 3 Å molecular sieves inside an argon filled glovebox. Lithium trifluoromethanesulfonate (LiOTf), sodium trifluoromethanesulfonate (NaOTf), tetraethyl trifluoromethanesulfonate (TEAOTf) and lithium chloride (LiCl) were purchased from Sigma Aldrich. All salts and solvents were stored in a glovebox and in addition, solutions and electrolytes were prepared in a glovebox. The water content of these solvents was tested using a Metrohm Karl Fischer Coulometer. Water content in these electrolytes was below 10 ppm. All measurements were conducted at room temperature; the voltammograms were obtained by scanning from the open circuit potential (OCP) to the oxygen reduction region then toward positive potentials where oxygen evolution reactions occur. IR spectra were collected over 30s while the electrode potential was varied with a 10 mV/s scan rate. SEIRA spectra were plotted as the relative change in the IR signal with respect to OCP using the formula,

$$\frac{\Delta S}{S} = \frac{S_{Variable} - S_{OCP}}{S_{OCP}}.$$

where S_{OCP} corresponds to signal obtained at OCP and $S_{variable}$ indicate signal obtained at various stages during CV. A negative going band in this case indicates an increasing absorbance when compared to the OCP reference state.

Electrochemical Measurements

Cyclic voltammetry (CV) was carried out in a three-electrode cell using a planar Au electrode as working electrode, Pt and Ag wire as counter and reference electrode respectively.

Computational methods

All structures were fully optimised using Gaussian09.[52] All structures except Na_2O_2 were calculated using CCSD(T)/6-311+G(3d,f).[53] Default settings were used apart from SCF=QC and INT=ULTRAFINE. Due to difficulties in completing the calculations Na_2O_2 was calculated using M06/6-311+G(3d,f).[54] Harmonic vibrational frequencies were computed for all optimized structures to verify that they were minima possessing zero imaginary frequencies.

Results and Discussions

In simple terms, the general mechanism of O_2 reduction in non-aqueous Li-O_2 and Na-O_2 batteries can be represented in the following chemical and electrochemical reactions:

$$\mathbf{O_{2(ads)} + e^- \rightleftharpoons O_{2\,(ads)}^-} \quad \mathbf{(1)}$$

$$\mathbf{O_{2(ads)}^- + M^+ \rightleftharpoons MO_{2(ads)}} \quad \mathbf{(2)}$$

$$\mathbf{MO_{2(ads)} \rightleftharpoons MO_{2(sol)}} \quad \mathbf{(3)}$$

$$\mathbf{2MO_{2(sol)} \rightleftharpoons M_2O_{2(sol)} + O_2} \quad \mathbf{(4)}$$

$$\mathbf{MO_{2(ads)} + e^- + M^+ \rightleftharpoons M_2O_{2(ads)}} \quad \mathbf{(5)}$$

$$\mathbf{M_2O_{2(ads)} \rightleftharpoons M_2O_{2(sol)}} \quad \mathbf{(6)}$$

In the above equations, M indicates alkali metal (Li or Na), "ads" indicated adsorbed species and "sol" indicates bulk/solubilized species. For both Li-O_2 and Na-O_2 batteries the first step is the reduction of oxygen to form superoxide (O_2^-) and in the presence of metal cation, a chemical step occurs to form MO_2 (i.e. LiO_2 or NaO_2). In general, the stability of alkali metal superoxide (MO_2) increases down the group, but the kinetic stability of MO_2 is also determined by the chemical and electrochemical environments. Depending on the conditions, the metastable MO_2 can follow either the chemical step (equation 4) or the electrochemical step (equation 5) to form M_2O_2. If the MO_2 intermediate is soluble in the electrolyte, then M_2O_2 is formed *via* a solution-mediated process, in contrast to surface-confined reaction in solvents that do not efficiently dissolve the superoxide intermediate. Well-documented reports in the area of Li-O_2 batteries suggest that Li_2O_2 is the primary discharge product in non-aqueous Li-O_2 cells, whereas both NaO_2 and Na_2O_2 have been

detected in Na-O_2 cells,[7, 55, 56] owing to the relative kinetic stability of NaO_2 compared to LiO_2. Recent studies demonstrated that the primary discharge products in M-O_2 batteries is also determined by the stability and solubility of MO_2 in the given (electro)chemical environment[22, 26]; the presence of water also affects the formation of discharge products[57, 58]. Using SEIRAS we investigate these mechanistic aspects of Li-O_2 and Na-O_2 chemistry in two different solvents, viz. DMSO and MeCN. Because no previous reports are available on the IR spectra of MO_2 or M_2O_2 in these environments, we intend to make an evaluation by comparing our results to the recent Raman spectro-electrochemistry studies in analogous systems. The assignment of bands and IR activity of these species are supported by our CCSD(T) calculations, as well as existing IR spectroscopy of superoxide species in isolated matrices.

In situ SEIRAS Characterization

Figure 2a shows a CV recorded in oxygen purged 0.1M LiOTf/DMSO electrolyte on an Au electrode at 10 mVs^{-1} scan rate. A negative going current peak at 2.63 V vs. Li/Li^+ indicates oxygen reduction forming O_2^- followed by Li_xO_y, and the positive peak at 3.5 V vs. Li/Li^+ corresponds to the oxidation of reduced species back to O_2 and Li^+. The SEIRA spectra were obtained simultaneously during the potential scan; corresponding spectra are shown in Figure 2b. For convenience, only the sections relevant to $\nu_{O\text{-}O}$ or $\nu_{Li\text{-}O}$ of LiO_2 and Li_2O_2 are shown here (see supplementary figure 1a for the SEIRA spectra over the entire 1700-700 cm^{-1} region). The black spectrum in Figure 2b corresponds to OCP (3.05 V vs. Li/Li^+), which shows no remarkable features because at OCP the interface was virtually undisturbed and no changes were observed in this spectrum with respect to the reference spectrum that was also obtained at the OCP. From the OCP the potential was scanned toward the negative vertex (1.6 V vs. Li/Li^+) and then to the positive vertex (3.9 V vs. Li/Li^+) before returning to the initial OCP. The spectra collected during this potential scan are

shown in Figure 2b, a major feature being the two peaks developed respectively at around 1127 cm^{-1} and 780 cm^{-1} as the electrode potential was scanned to negative values from OCP. The position of these bands matches closely with that of LiO_2 and Li_2O_2 typically observed using Raman spectroscopy. Calculations (CCSD(T)/6-311+G(3d,f).) assign these bands to LiO_2 (ν_{O-O} 1127 cm^{-1}) and Li_2O_2 ((ν_{Li-O} 826 cm^{-1}); these bands are IR active when the species are in their molecular forms. In order to rule out the appearance of these bands from the changing surface interaction of salt LiOTf, the experiment was repeated using the salt LiCl. SEIRAS corresponding to oxygen reduction in DMSO/LiCl electrolyte also shows analogous superoxide and peroxide bands (SI Figure 11).

Table 1 Comparison of Experimental and Calculated IR active Harmonic Frequencies (cm^{-1}). [a]Full list of calculated harmonic frequencies found in SI

	Experiment	**Calculation**	**Literature** (matrix isolation studies)
	(cm^{-1})	**(cm^{-1})**	**(cm^{-1})**
Li_2O_2	780, 830	826[a] (ν_{Li-O})	767-872[33]
LiO_2	1127-1139	1130[a] (ν_{O-O})	1097[30, 32], 1127[32]
Na_2O_2	-	590[a] (ν_{Na-O})	-
NaO_2	1122-1125	1166[a] (ν_{O-O})	1080[31], 1112[31]
H_2O_2	895 – 905	911[a] (ν_{O-O})	
HO_2^-	-	756[a] (ν_{O-O})	
HO_2^-	-	1164[a] (δ_{H-O-O})	
LiOOH	1170	1176[a] (δ_{H-O-O})	

In fact, there have been some reports on the IR activity of molecular LiO_2 and Li_2O_2 from matrix isolation studies,[30-33] but IR active bands within the wavenumber range accessible through the ZnSe prism are generally not to be expected for crystalline Li_2O_2, where bands are typically observed at 530, 422, and 337 cm^{-1}.[17, 59] These factors present a rationale for the observation of molecular LiO_2 and Li_2O_2 species in our system. Bruce *et al.* proposed that high donor number solvents (DMSO for example) promote discharge product formation *via* a solvent mediated route.[15] The IR active bands corresponding to molecular LiO_2 or Li_2O_2 species observed here could indicate metastable species formed during this solvent mediated discharge product formation. Once these LiO_2 or Li_2O_2 molecular species are transformed into solid crystalline phases or surface films, their corresponding $\nu_{O\text{-}O}$ or $\nu_{Li\text{-}O}$ would no longer be IR active in the range assessable using the ZnSe window >700 cm^{-1} (IR active bands for crystalline Li_2O_2 are observable at 530, 422 and 337 cm^{-1}),[17] although Raman bands will remain active. Our observation of these peaks strongly supports the notion that DMSO promotes the formation of discrete molecules of reduced oxygen species. Significantly, this result is direct proof of the presence of molecular Li_2O_2 at the electrode interfacial region. Raman spectroscopy cannot distinguish spectroscopically between bulk and molecular Li_2O_2, whereas IR is only sensitive to molecular Li_2O_2. An alternative, but less likely, scenario is that a large number of small clusters or crystallites of insoluble Li_2O_2 form at the interface, with symmetry breaking at their surface giving apparent IR activity to only the peripheral Li_2O_2. However, the results presented later in the manuscript for MeCN electrolytes also support the notion that the IR bands are indeed from molecular Li_2O_2 in solution.

It is also worth noting that the IR bands, particularly the Li_2O_2 band, do not disappear at the positive potentials, meaning there is still Li_2O_2 (and even small amounts of LiO_2) present close enough to the interface to be detected by SEIRAS during the timescale of the experiment. In addition to

the two major IR bands, two weak bands around 830 cm^{-1} and 853 cm^{-1} starts to appear and the 853 cm^{-1} band appears more pronounced after the oxidation peak in the CV. These bands could be related to protonated peroxides or other forms or higher-order Li_xO_y molecular clusters or any undesirable reaction products or intermediates.[60, 61] Although computational studies employed in this report established the IR activity of low order molecular Li_xO_y species, theoretical studies exploring other possible Li_xO_y clusters and the contribution of solvent interaction with them would be necessary in order to accurately assign these band positions. Further studies are underway to explore this. None of these bands were observed in deoxygenated DMSO/LiOTf systems (please find details in the supporting figure S4a) indicating that all the peaks discussed here relate to desirable or undesirable ORR products or intermediates. In addition to the bands related to the reduced oxygen species discussed above, we also observe some bands (major bands positioned around 1440 cm^{-1}, 1410 cm^{-1}, 1310 cm^{-1}, 1245 cm^{-1}, 1230 cm^{-1} and 1060 cm^{-1}) appearing upon potential scan which do not appear "reversible" upon return to OCP. The position of these bands match well with the bands of the electrolyte components (please see Table S8), considering that small shifts in band positions are expected for species near the electrode surface. The apparent irreversibility of these bands is related to potential induced changes in the very thin gold layer (20 nm) formed on the ATR prism, which alters absorbance of the species present at the interface. While a thin gold nanoisland film used here helps with the detection of reduced oxygen species, this technical issue limits any quantitative analysis based on the absorbance obtained.

Figures 3a and 3b show a CV and corresponding SEIRA spectra respectively for 0.1 M NaOTf/ DMSO electrolyte on Au (see supplementary figure 1b for the SEIRA spectra recorded over the entire region). A band at 1122 cm^{-1} appears as the potential is scanned toward negative values. This process is apparently electrochemically reversible in this case as the corresponding peak disappears at positive potentials. The position of this band is close to what we observed for LiO_2,

which would indicate that this band corresponds to NaO_2 in this case, but the calculated harmonic frequency of NaO_2 is apparently 41 cm^{-1} higher. The chemical or electrochemical environment of the superoxide species will have subtle influences on the degree of charge transfer to their O-O bond. Extensive computational studies taking higher order molecular clusters of these species, as well as solvent coordination also into consideration would be necessary to establish precise assignments of these bands; studies to address this possibility are currently underway in our group. A major difference between the NaO_2 and LiO_2 spectroscopic peaks (Figures 2 and 3) is that the IR band observed for LiO_2 does not completely reversibly disappear even at the most positive potential, whereas the band corresponds to NaO_2 completely disappears at positive potentials. Interestingly, a significant electrode potential dependent shift in the LiO_2 band (-9 cm^{-1}/V) was also observed, while the shift is relatively small for the NaO_2 peak (-4 cm^{-1}/V). Electrode potential dependent wavenumber shifts could have a variety of origins; they could be due to the interaction of the dipole with the intense electric field at the interface or the shifts could be due to electrode potential dependent changes in charge transfer between the electrode and an adsorbate. More subtle effects could include electrode potential dependent changes in solvation or interactions with charged species in the interfacial region. The observed larger shift in the LiO_2 system could indicate a stronger interaction of LiO_2 with the surface or the electric field of the electrochemical double layer when compared to NaO_2 system. Even though the coordination of DMSO assists in the formation of discrete LiO_2 species, LiO_2 would still have to maintain a strong interaction with the surface or electric field of the electrochemical double layer to exhibit appreciable electrode potential dependent wavenumber shifts. Conversely smaller shifts in the case of NaO_2 might point to a weaker interaction with the surface or interfacial field. A recent report addressing the mechanistic oxygen reduction in Li^+ containing DMSO indicates that the formation of Li_2O_2 on gold electrode proceeds mainly *via* electrochemical reduction (equation (5) above) rather than chemical disproportionation (equation (4) above) in the bulk.[62] This indicates that DMSO solvated LiO_2 is within close vicinity of the gold electrode. However, since the electrode potential dependence of vibrational bands can have several origins it is not possible to definitively attribute the larger wavenumber shift for the LiO_2 band to a stronger interaction with the surface.

In contrast to the observation for the Li-O_2 system (Figure 2a), we do not see any bands in the 780 cm^{-1} - 860 cm^{-1} region in Na-O_2 system (Figure 3b). However, this does not necessarily rule out

the possibility of Na_2O_2 formation in this system, as our computation studies suggest that the Na_2O_2 IR band would appear below 700 cm^{-1} (see supporting information, table S3), which is difficult to observe with our present setup using ZnSe ATR elements and MCT detector. Spectra resulting from the control experiments in argon purged 0.1 M NaOTf/ DMSO electrolyte are provided in the supporting information.

An analogous set of measurements were carried out in MeCN-based electrolytes as well. In these measurements in MeCN, it proved very difficult to detect the superoxide as well as peroxide bands, in comparison to DMSO. These corresponding spectra recorded for electrolyte solutions containing 0.1 M LiOTf or 0.1 M NaOTf are shown in the supporting information Figures S4 and S5. We believe the lack of corresponding $\nu_{O\text{-}O}$ IR bands in the MeCN-based electrolytes is due to the absence or low concentration of solvent coordinated discrete MO_2 molecular species in this electrolyte, however a very weak band at ca 800 cm^{-1} (ν Li-O) may suggest the presence of Li_2O_2 (Figure S4). The solvation of ORR products (as in the case of DMSO) is apparently crucial for the IR activity of these species. The difference in solvation of the discharge products between DMSO and MeCN is linked to their donor number (which is a quantitative measure of Lewis basicity), 29.8 kcal/mol and 14.1 kcal/mol respectively. This observation is in line with the solvent dependent ORR mechanisms postulated in recent reports.[22, 24-26, 55] In order to examine this further, we carried out measurements in MeCN containing low concentrations (5 mM) of LiOTf or NaOTf. In order to maintain a reasonable ionic conductivity of the electrolyte 95 mM TEAOTf was included as the supporting salt. Comparable $\nu_{O\text{-}O}$ corresponding to both NaO_2 and LiO_2 were observed in both these cases (Figures 4 and 5). Notably, in addition to the peaks observed in DMSO based electrolytes containing either LiOTf or NaOTf only (at 1127 cm^{-1} and 1122 cm^{-1} respectively), an additional peak at a lower wavenumber (~1100 cm^{-1}) was also observed in this case. This low frequency

band could correspond to more weakly coordinated superoxide, such as the species $TEA^+O_2^-$. This latter species is typically observed using Raman spectroscopy when there is tetraalkylammonium salts present in the electrolyte instead of an alkali metal cation. Another notable point is that there is no significant Stark shift of the LiO_2 or the NaO_2 peaks in this case. This contrasts with our observations for the DMSO/0.1 M LiOTf electrolyte, where a considerable Stark shift of the LiO_2 band is apparent. This might suggest that in the presence of TEA^+, the Li_xO_y species are formed further away from the surface, i.e. out of the influence of the electric field of the electrochemical double layer and not directly surface attached. In this case the tetraalkylammonium cation additive might be acting as a phase transfer catalyst as has been suggested previously[63, 64]. Because of the presence of a phase transfer agent, the reduced oxygen species would not directly interact with the surface and thus no Stark shift would be observed in this case. Corresponding control experiments in argon-purged electrolytes are presented in the supporting information (Supporting Figures S7 and S8).

The presence of water has a detrimental effect in non-aqueous M-O_2 batteries. In DMSO/LiOTf, when slightly contaminated with water (> 50 ppm), we observed additional peaks, notably around 1154 cm^{-1}, 1170 cm^{-1} and 1500 cm^{-1} (Supporting Figure S10). Our CCSD calculations suggests that the 1170 cm^{-1} band can be related to the $\delta_{H\text{-}O\text{-}O}$ mode of HO_2^- or LiO_2H. We have tentatively assigned this band to LiO_2H (please see Table 1) in the light of a recent empirical evidence demonstrating the absence of a band around this wavenumber for HO_2^- in aqueous medium,[35] though we do not completely rule out this possibility as the effect of solvation would be significantly different in our non-aqueous system. The 1154 cm^{-1} band appears only at positive potential which is in agreement with the formation of dimethyl sulfone reported by other groups, indicating that the

presence of trace water promotes this side reaction[43]. The 1500 cm^{-1} peak indicates that inorganic carbonates are also formed under these compromised conditions.

Our ATR-SEIRAS studies comparing Li-O_2 and Na-O_2 electrochemistry in DMSO and MeCN provide important information about the ORR mechanism through the direct spectroscopic detection of reduced oxygen species. IR activity of these species is strongly dependent on the electrolyte composition as well as the donicity of the solvent. A qualitative evaluation highlighting the strong dependence of the ORR reactions on the solvent as well as the metal is shown in Figure 6. Insights obtained from our SEIRAS studies help to explain the differences between CVs shown in Figure 6. The first reduction peak observed in all the CVs corresponds to the formation of superoxide by the reduction of molecular oxygen. In DMSO based electrolytes, both Li-O_2 and Na-O_2 systems show moderate peak-to-peak separation in the CVs of the superoxide electrochemistry (black curves in Figure 6a and Figure 6b respectively). However, after sweeping more cathodic to the peroxide formation step (second reduction peak in the voltammograms), a significantly higher overpotential for oxidation of DMSO/Li^+ compared to DMSO/Na^+ is observed in the anodic sweep (Figures 6a and 6b, red curves). Our SEIRAS results (Figure 2a) suggest that the IR bands corresponding to ORR products formed in DMSO/Li^+ are not completely re-oxidised presumably due to kinetic factor, whereas ORR in DMSO/Na^+ gives more facile oxidation of the ORR products. This difference in the reduction/reoxidation electrochemistry observed in in the IR spectra is also apparent in the CVs. Interestingly, in MeCN, both the Li^+ and Na^+ systems show large reduction overpotentials when the electrode potential is scanned further negative to form the peroxide species (Figures 6c and 6d, red curves). This observation for MeCN highlights that the dramatic difference in overpotentials between the Li^+ and Na^+ systems in DMSO is not due to the difference in coordination alone, but it is strongly influenced by the ORR mechanism. The solvent plays a significant

role in determining which mechanism is followed; i.e. whether the solution mediated or surface confined pathway. In MeCN even the superoxide oxidation electrochemistry (Figures 6c and 6d, black curves) shows a large overpotential compared to the DMSO system, indicating that even the first reduction step to superoxide follows a surface confined route leading to the direct deposition. Therefore, the formation of a surface film of LiO_2 or NaO_2 *via* a surface mediated reaction in MeCN is highly likely.

The CVs shown in Figure 7 summarize the significant changes in the cyclability and reversibility discussed in the previous section. In DMSO/NaOTf system, both superoxide and peroxide formation steps are solution mediated processes, whereas in DMSO/LiOTf, peroxide is formed on the surface and hence due to sluggish kinetics the discharge species formed on the electrodes surface are not effectively removed therefore CV scans diminish significantly over 20 cycles (Figure 7a). By contrast, the DMSO/NaOTf redox chemistry is stable (Figure 7b), because of the solution mediation and formation of superoxide in solution. Consistent with our spectroscopic observation, even the first reduction step (superoxide formation) follows a surface confined route in MeCN; the CV in Figure 7c shows diminishing ORR/OER peaks upon cycling in MeCN/NaOTf electrolyte despite limiting the lower vertex potential to 2.1V.

Conclusions

An *in situ* ATR-SEIRAS based approach for the detection for the ORR species in model systems relevant to M-O_2 batteries have been demonstrated. Our IR studies combined with CCSD (T) calculations show that the electrolyte composition has a strong influence on the IR activity of the discharge species. We have demonstrated that the $\nu_{O\text{-}O}$ of alkali metal superoxides (LiO_2 and NaO_2) and $\nu_{Li\text{-}O}$ of lithium metal peroxides are IR active in electrolytes composed of DMSO and a metal salt (LiOTf or NaOTf). Importantly, SEIRAS provides direct experimental proof that molecular "Li_2O_2" is present at the electrode interface. The effect of electrolyte components on the IR activity of the discharge species proposes SEIRAS as a powerful methodology for selective detection of solubilized molecular species of dioxygen reduction products formed in non-aqueous electrolytes. Our *in situ* SEIRAS approach will aid the differentiation between the surface and solvent mediated routes for the discharge product formation in non-aqueous M-O_2 batteries and support ongoing efforts towards understanding mechanistic pathways at the cathode.

ASSOCIATED CONTENT

Supporting Information. "This material is available free of charge *via* the Internet at http://pubs.acs.org"

Details of ATR-SEIRAS setup, additional SEIRA spectra and electrochemical data, IR band assignments, ATR spectra of relevant salts and solvents, computational methods and calculations

AUTHOR INFORMATION

Corresponding Author

*hardwick@liverpool.ac.uk

ACKNOWLEDGMENT

We acknowledge the Engineering and Physical Sciences Research Council (EPSRC) for the funding of this research under Grant Numbers EP/K006835/1 and EP/K016954/1. The authors would like to thank Georgios Papageorgiou and Prof. Ken Durose (University of Liverpool) for the use of the thermal evaporator.

Figures

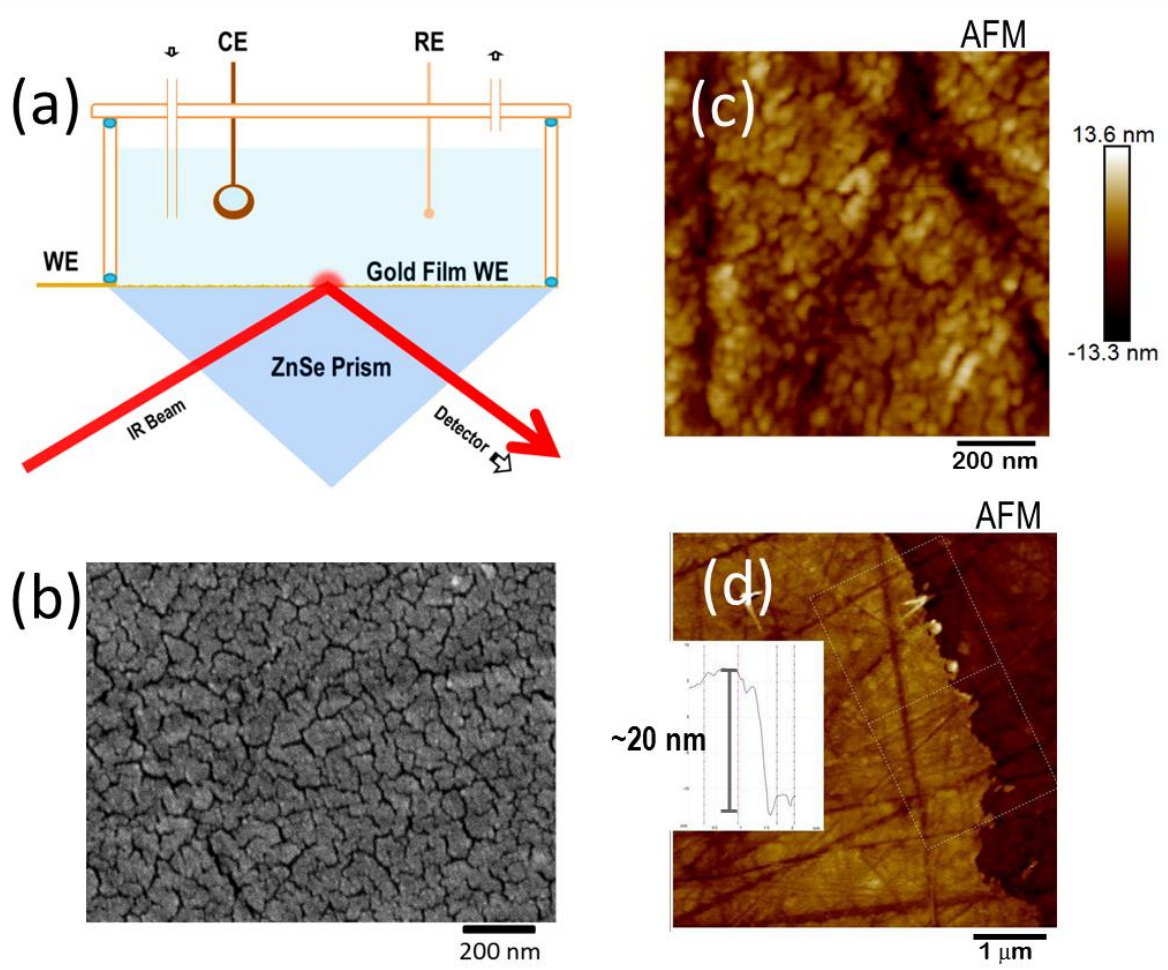

FIGURE 1.

1a: Sketch of the experimental setup for ATR-SEIRAS spectroelectrochemical cell

1b: SEM of the gold film formed on a ZnSe surface

1c, 1d: AFM images showing structure, morphology and thickness of the gold island film formed on the prism

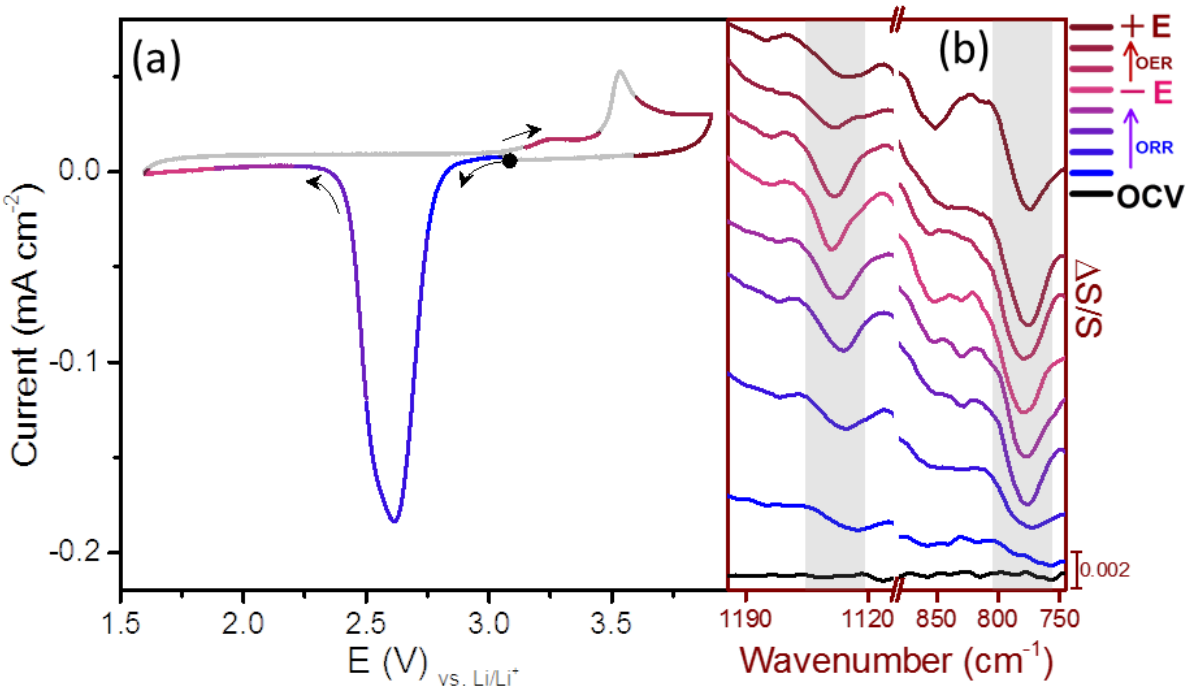

FIGURE 2. CV of ORR/OER at 10 mV/s scan rate in O_2 purged 0.1 M LiOTf in DMSO on a Au electrode (a) and corresponding *in situ* SEIRA spectra (b). Spectrum at the bottom was collected at the OCP and those acquired at different stages during potential sweep are color-coded to match different regions in the CV. Grey shadings show the region where LiO_2 or Li_2O_2 bands are observed. As explained in the experimental section, a negative going band corresponds to an increasing absorbance when compared to the OCP reference state (this applies for subsequent spectra too).

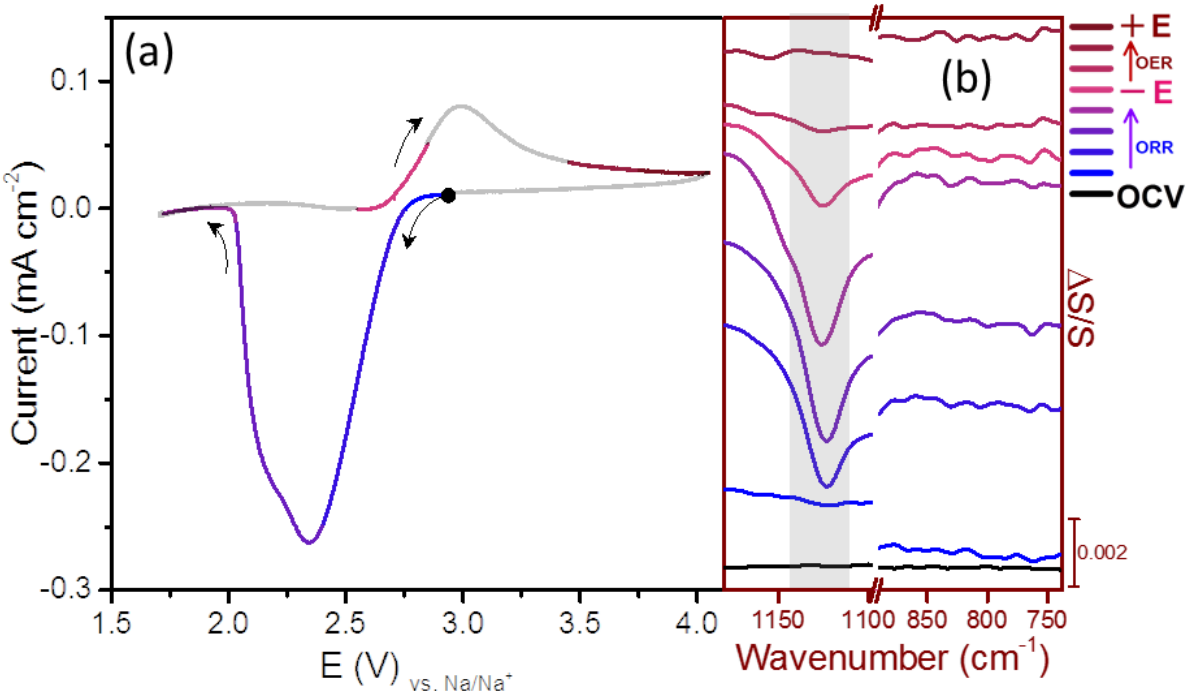

FIGURE 3. CV of ORR/OER at 10 mV/s scan rate in O_2 purged 0.1 M NaOTf in DMSO on a Au electrode (a) and corresponding *in situ* SEIRA spectra (b). Spectrum at the bottom was collected at the OCP and those acquired at different stages during potential sweep are color-coded to match different regions in the CV. Grey shading shows the region where NaO_2 bands are observed.

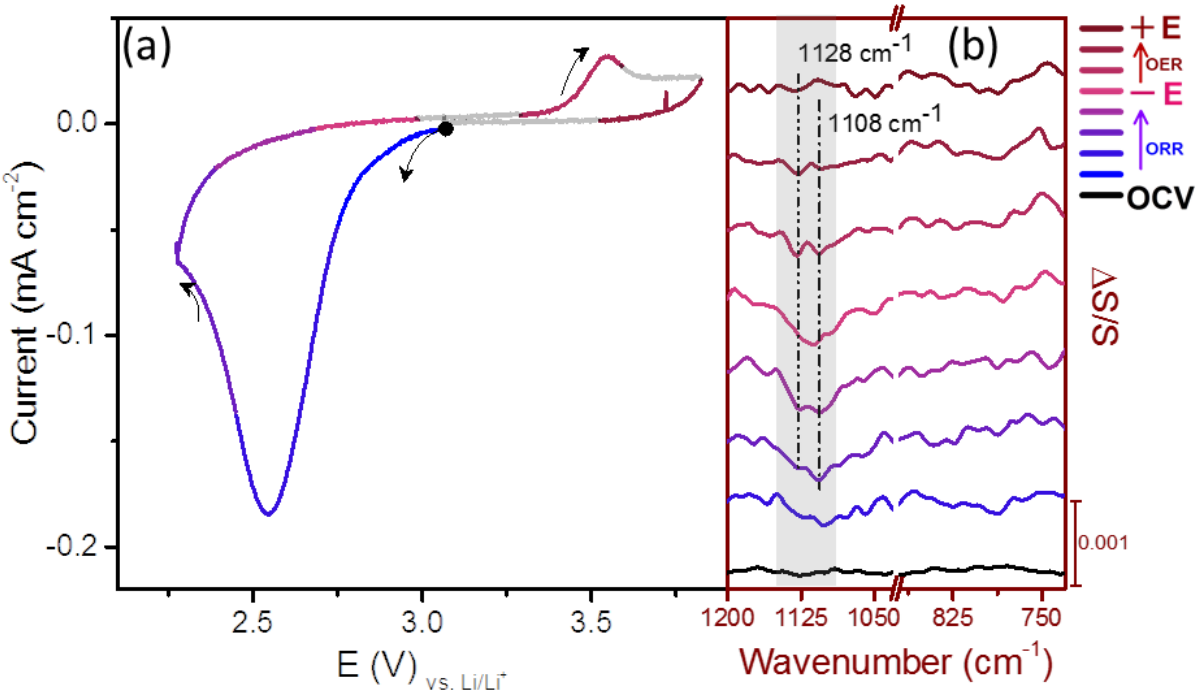

FIGURE 4. CV of ORR/OER at 10 mV/s scan rate in O_2 purged 0.005 M LiOTf + 0.095 M TEAOTf in MeCN on a Au electrode (a) and corresponding *in situ* SEIRA spectra (b). Spectrum at the bottom was collected at the OCP and those acquired at different stages during potential sweep are color-coded to match different regions in the CV. Vertical dotted lines in the grey shading show the doublet character of the superoxide band.

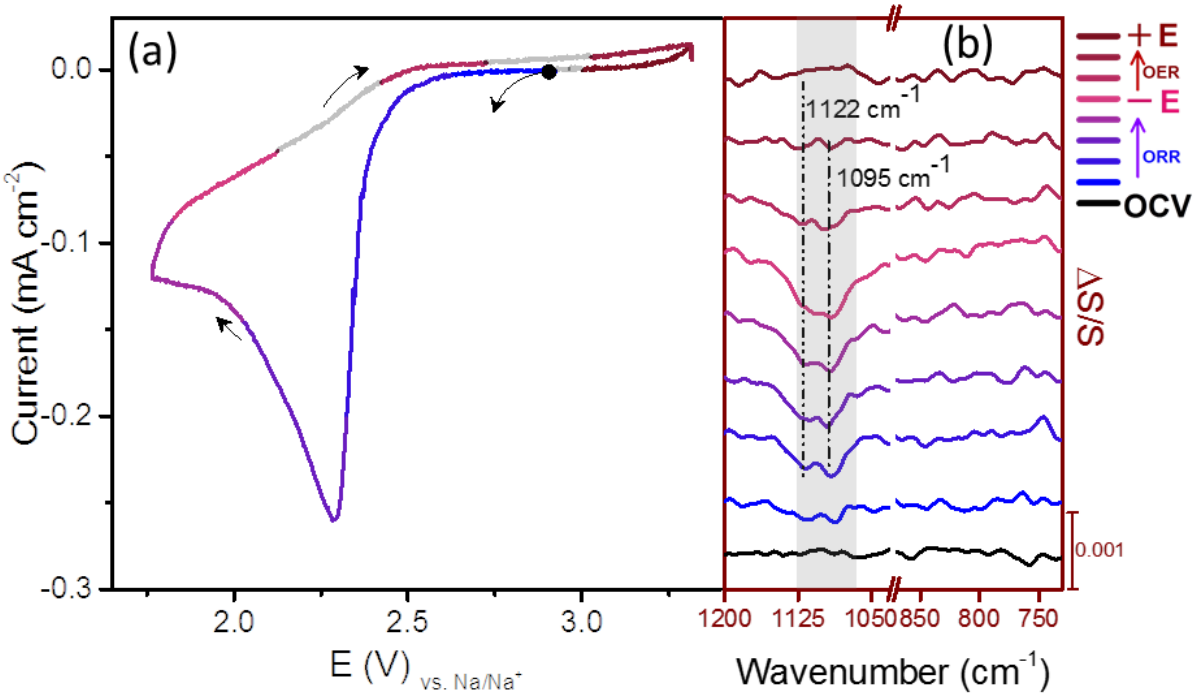

FIGURE 5. CV of ORR/OER at 10 mV/s in O_2 purged 0.005 M NaOTf + 0.095 M TEAOTf in MeCN on Au electrode (a) and corresponding *in situ* SEIRA spectra (b). Spectrum at the bottom was collected at the OCP and those acquired at different stages during potential sweep are color-coded to match different regions in the CV. Vertical dotted lines in the grey shading show the doublet character of the superoxide band.

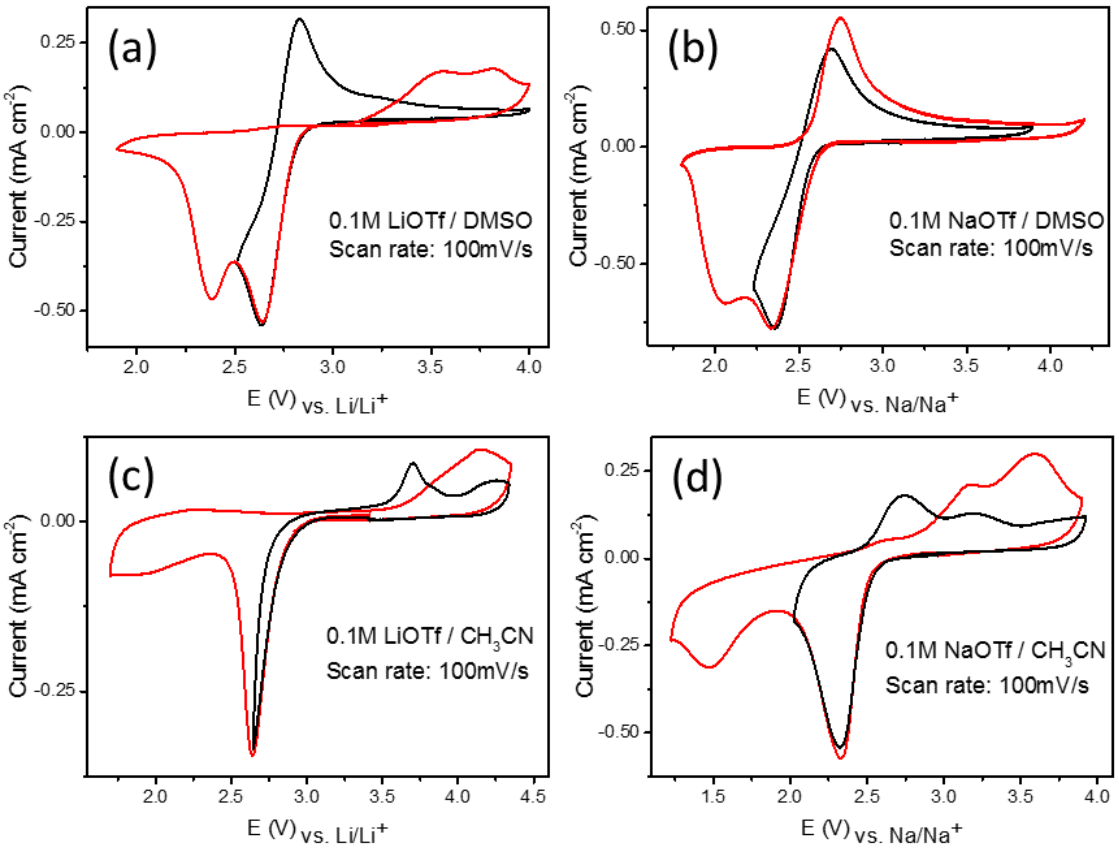

FIGURE 6. CVs obtained on a Au electrode at 100 mV/s scan rate for four different electrolyte compositions. Electrolytes are composed of either DMSO (a and b) or MeCN (c and d) as the solvent and either 0.1 M LiOTf (a and c) or 0.1 M NaOTf (b and d) as the salt. Black CVs show cycles when the lower vertex was limited to the first reduction, while the red CVs show cycles when the potential was swept through both reduction peaks.

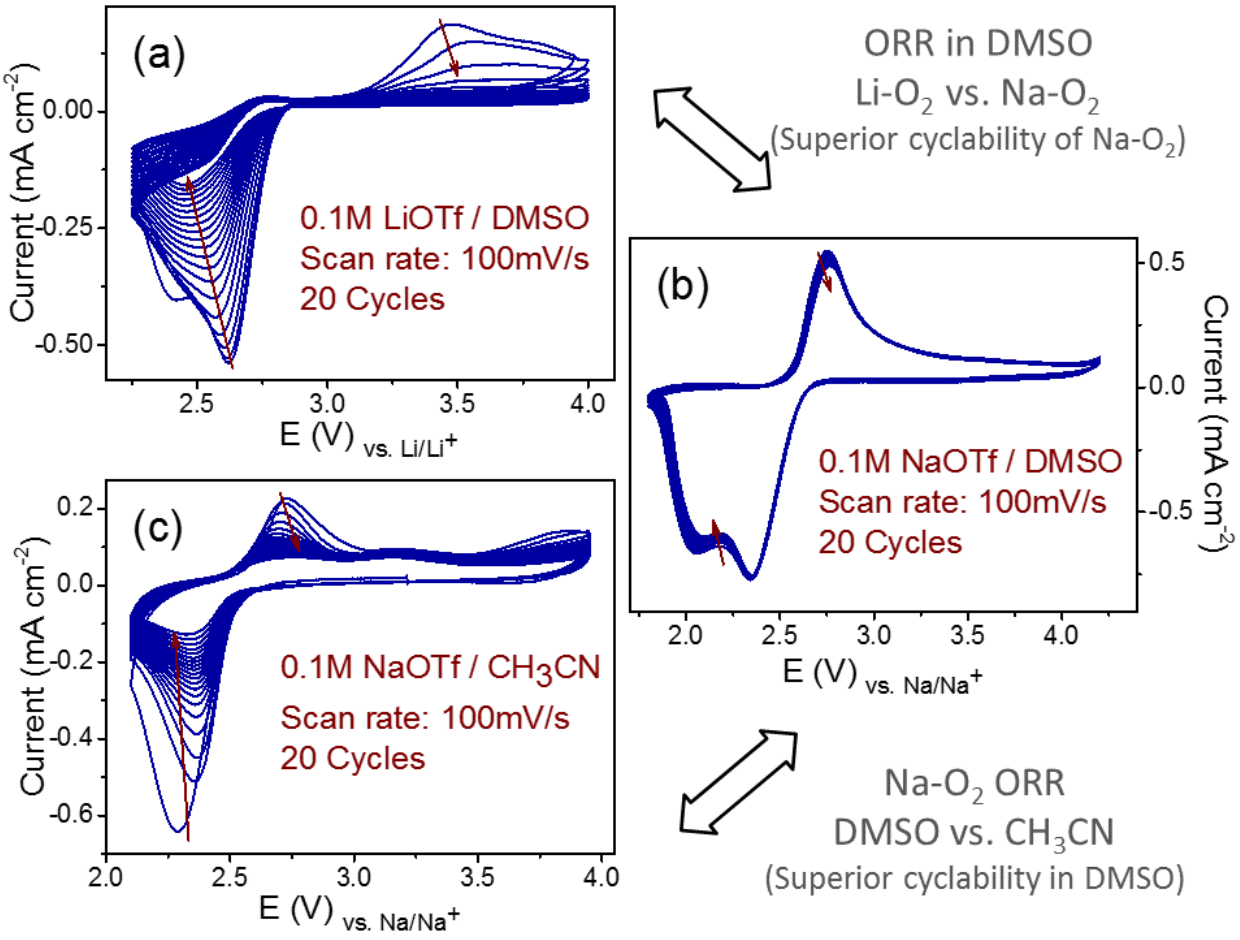

FIGURE 7. CVs obtained at 100 mV/s scan rate on a Au electrode at three different electrolyte compositions: (a) 0.1 M LiOTf in DMSO (b) 0.1 M NaOTf in DMSO (c) 0.1 M NaOTf in MeCN. Figures a and b compares the effect of Li^+/Na^+ on the ORR/OER cyclability in the same solvent. Figures b and c compares the effect of solvent (DMSO vs. MeCN) at the same salt composition.

REFERENCES

1. Bruce, P. G.; Freunberger, S. A.; Hardwick, L. J.; Tarascon, J.-M., Li-O_2 and Li-S with high energy storage. *Nature Materials* **2012,** *11* (1), 19-29.
2. Aurbach, D.; McCloskey, B. D.; Nazar, L. F.; Bruce, P. G., Advances in understanding mechanisms underpinning lithium–air batteries. **2016,** *1*, 16128.
3. Luntz, A. C.; McCloskey, B. D., Nonaqueous Li–air batteries: a status report. *Chem. Rev.* **2014,** *114* (23), 11721-11750.
4. Garcia-Araez, N.; Novak, P., Critical aspects in the development of lithium-air batteries. *Journal of Solid State Electrochemistry* **2013,** *17* (7), 1793-1807.
5. Black, R.; Adams, B.; Nazar, L. F., Non-aqueous and hybrid Li-O_2 batteries. *Adv. Energy Mater.* **2012,** *2* (7), 801-815.
6. Girishkumar, G.; McCloskey, B.; Luntz, A. C.; Swanson, S.; Wilcke, W., Lithium-air battery: promise and challenges. *Journal of Physical Chemistry Letters* **2010,** *1* (14), 2193-2203.
7. Aetukuri, N. B.; McCloskey, B. D.; Garcia, J. M.; Krupp, L. E.; Viswanathan, V.; Luntz, A. C., Solvating additives drive solution-mediated electrochemistry and enhance toroid growth in non-aqueous Li-O-2 batteries. *Nat. Chem.* **2015,** *7* (1), 50-56.
8. Feng, N. N.; He, P.; Zhou, H. S., Critical challenges in rechargeable aprotic Li-O_2 batteries. *Adv. Energy Mater.* **2016,** *6* (9), 24.
9. Grande, L.; Paillard, E.; Hassoun, J.; Park, J. B.; Lee, Y. J.; Sun, Y. K.; Passerini, S.; Scrosati, B., The lithium/air battery: still an emerging system or a practical reality? *Adv. Mater.* **2015,** *27* (5), 784-800.
10. Bruce, P. G.; Freunberger, S. A.; Hardwick, L. J.; Peng, Z. Q.; Chen, Y. H., Lithium-air battery. *Abstr. Pap. Am. Chem. Soc.* **2010,** *240*, 1.
11. Lu, J.; Jung Lee, Y.; Luo, X.; Chun Lau, K.; Asadi, M.; Wang, H.-H.; Brombosz, S.; Wen, J.; Zhai, D.; Chen, Z.; Miller, D. J.; Sub Jeong, Y.; Park, J.-B.; Zak Fang, Z.; Kumar, B.; Salehi-Khojin, A.; Sun, Y.-K.; Curtiss, L. A.; Amine, K., A lithium–oxygen battery based on lithium superoxide. *Nature* **2016,** *529* (7586), 377-382.
12. Zhang, T.; Zhou, H., A reversible long-life lithium-air battery in ambient air. *Nature Communications* **2013,** *4*.

13. Xu, J.-J.; Wang, Z.-L.; Xu, D.; Zhang, L.-L.; Zhang, X.-B., Tailoring deposition and morphology of discharge products towards high-rate and long-life lithium-oxygen batteries. *Nature Communications* **2013,** *4*, 2438.
14. Liu, T.; Leskes, M.; Yu, W.; Moore, A. J.; Zhou, L.; Bayley, P. M.; Kim, G.; Grey, C. P., Cycling Li-O_2 batteries via LiOH formation and decomposition. *Science* **2015,** *350* (6260), 530-533.
15. Hartmann, P.; Bender, C. L.; Vracar, M.; Durr, A. K.; Garsuch, A.; Janek, J.; Adelhelm, P., A rechargeable room-temperature sodium superoxide (NaO_2) battery. *Nature Materials* **2013,** *12* (3), 228-232.
16. Xia, C.; Black, R.; Fernandes, R.; Adams, B.; Nazar, L. F., The critical role of phase-transfer catalysis in aprotic sodium oxygen batteries. *Nat. Chem.* **2015,** *7* (6), 496-501.
17. Freunberger, S. A.; Chen, Y. H.; Peng, Z. Q.; Griffin, J. M.; Hardwick, L. J.; Barde, F.; Novak, P.; Bruce, P. G., Reactions in the rechargeable lithium-O_2 battery with alkyl carbonate electrolytes. *J. Am. Chem. Soc.* **2011,** *133* (20), 8040-8047.
18. Freunberger, S. A.; Chen, Y.; Drewett, N. E.; Hardwick, L. J.; Bardé, F.; Bruce, P. G., The lithium–oxygen battery with ether-based electrolytes. *Angewandte Chemie International Edition* **2011,** *50* (37), 8609-8613.
19. McCloskey, B. D.; Speidel, A.; Scheffler, R.; Miller, D. C.; Viswanathan, V.; Hummelshøj, J. S.; Nørskov, J. K.; Luntz, A. C., Twin problems of interfacial carbonate formation in nonaqueous Li–O_2 batteries. *The Journal of Physical Chemistry Letters* **2012,** *3* (8), 997-1001.
20. Black, R.; Oh, S. H.; Lee, J.-H.; Yim, T.; Adams, B.; Nazar, L. F., Screening for superoxide reactivity in Li-O_2 batteries: Effect on Li2O2/LiOH Crystallization. *J. Am. Chem. Soc.* **2012,** *134* (6), 2902-2905.
21. Kim, J.; Lim, H.-D.; Gwon, H.; Kang, K., Sodium-oxygen batteries with alkyl-carbonate and ether based electrolytes. *Physical Chemistry Chemical Physics* **2013,** *15* (10), 3623-3629.
22. Johnson, L.; Li, C. M.; Liu, Z.; Chen, Y. H.; Freunberger, S. A.; Ashok, P. C.; Praveen, B. B.; Dholakia, K.; Tarascon, J. M.; Bruce, P. G., The role of LiO_2 solubility in O_2 reduction in aprotic solvents and its consequences for Li-O_2 batteries. *Nat. Chem.* **2014,** *6* (12), 1091-1099.

23. Peng, Z.; Freunberger, S. A.; Hardwick, L. J.; Chen, Y.; Giordani, V.; Barde, F.; Novak, P.; Graham, D.; Tarascon, J.-M.; Bruce, P. G., Oxygen reactions in a Non-aqueous Li^+ electrolyte. *Angew. Chem.-Int. Edit.* **2011,** *50* (28), 6351-6355.

24. Abraham, K. M., Electrolyte-directed reactions of the oxygen electrode in lithium-air batteries. *Journal of the Electrochemical Society* **2015,** *162* (2), A3021-A3031.

25. Kwabi, D. G.; Bryantsev, V. S.; Batcho, T. P.; Itkis, D. M.; Thompson, C. V.; Shao-Horn, Y., Experimental and Ccomputational analysis of the solvent-dependent O_2/Li^+-O_2^- redox couple: standard potentials, coupling strength, and implications for lithium-oxygen batteries. *Angew. Chem.-Int. Edit.* **2016,** *55* (9), 3129-3134.

26. Aldous, I. M.; Hardwick, L. J., Solvent-mediated control of the electrochemical discharge products of non-aqueous sodium-oxygen electrochemistry. *Angew. Chem.-Int. Edit.* **2016,** *55* (29), 8254-8257.

27. Frith, J. T.; Russell, A. E.; Garcia-Araez, N.; Owen, J. R., An in-situ Raman study of the oxygen reduction reaction in ionic liquids. *Electrochemistry Communications* **2014,** *46*, 33-35.

28. Gittleson, F. S.; Yao, K. P. C.; Kwabi, D. G.; Sayed, S. Y.; Ryu, W. H.; Shao-Horn, Y.; Taylor, A. D., Raman spectroscopy in lithium-oxygen battery systems. *Chemelectrochem* **2015,** *2* (10), 1446-1457.

29. Streich, D.; Novák, P., Electrode-electrolyte interface characterization of carbon e lectrodes in Li-O_2 batteries: capabilities and limitations of infrared spectroscopy. *Electrochimica Acta* **2016,** *190*, 753-757.

30. Andrews, L., Matrix infrared spectrum and bonding in lithium superoxide molecule liO_2. *J. Am. Chem. Soc.* **1968,** *90* (26), 7368-&.

31. Andrews, L., Infrared spectra and bonding in the sodium superoxide and sodium peroxide molecules. *The Journal of Physical Chemistry* **1969,** *73* (11), 3922-3928.

32. Andrews, L., Infrared spectrum, structure, vibrational potential function, and bonding in the lithium superoxide molecule LiO_2. *The Journal of Chemical Physics* **1969,** *50* (10), 4288-4299.

33. Wang, X.; Andrews, L., Infrared spectra, structure and bonding in the LiO_2, LiO_2Li, LiO and Li_2O molecules in solid neon. *Molecular Physics* **2009,** *107* (8-12), 739-748.

34. Shao, M. H.; Liu, P.; Adzic, R. R., Superoxide anion is the intermediate in the oxygen reduction reaction on platinum electrodes. *J. Am. Chem. Soc.* **2006,** *128* (23), 7408-7409.
35. Nayak, S.; Biedermann, P. U.; Stratmann, M.; Erbe, A., A mechanistic study of the electrochemical oxygen reduction on the model semiconductor n-Ge(100) by ATR-IR and DFT. *Physical Chemistry Chemical Physics* **2013,** *15* (16), 5771-5781.
36. Ohta, N.; Nomura, K.; Yagi, I., Adsorption and electroreduction of oxygen on gold in acidic media: in situ spectroscopic identification of adsorbed molecular oxygen and hydrogen superoxide. *The Journal of Physical Chemistry C* **2012,** *116* (27), 14390-14400.
37. Kwabi, D. G.; Tulodziecki, M.; Pour, N.; Itkis, D. M.; Thompson, C. V.; Shao-Horn, Y., Controlling solution-mediated reaction mechanisms of oxygen reduction using potential and solvent for aprotic lithium-oxygen batteries. *Journal of Physical Chemistry Letters* **2016,** *7* (7), 1204-1212.
38. Sharon, D.; Etacheri, V.; Garsuch, A.; Afri, M.; Frimer, A. A.; Aurbach, D., On the Challenge of electrolyte solutions for Li-air batteries: monitoring oxygen reduction and related reactions in polyether solutions by spectroscopy and EQCM. *Journal of Physical Chemistry Letters* **2013,** *4* (1), 127-131.
39. Wandt, J.; Jakes, P.; Granwehr, J.; Gasteiger, H. A.; Eichel, R. A., Singlet Oxygen formation during the charging process of an aprotic lithium-oxygen battery. *Angew. Chem.-Int. Edit.* **2016,** *55* (24), 6892-6895.
40. Lau, K. C.; Lu, J.; Luo, X. Y.; Curtiss, L. A.; Amine, K., Implications of the unpaired spins in Li-O_2 battery chemistry and electrochemistry: a minireview. *ChemPlusChem* **2015,** *80* (2), 336-+.
41. Galloway, T. A.; Cabo-Fernandez, L.; Aldous, I.; Braga, F.; Hardwick, L., Shell isolated nanoparticles for enhanced raman spectroscopy studies in lithium-oxygen cells. *Faraday Discussions* **2017**.
42. Radjenovic, P.; Hardwick, L., Time-resolved SERS study of the oxygen reduction reaction in ionic liquid electrolytes for non-aqueous lithium-oxygen cells. *Faraday Discussions* **2017**.

43. Mozhzhukhina, N.; De Leo, L. P. M.; Calvo, E. J., Infrared Spectroscopy Studies on stability of dimethyl sulfoxide for application in a li-air battery. *J. Phys. Chem. C* **2013,** *117* (36), 18375-18380.
44. Vivek, J. P.; Berry, N.; Papageorgiou, G.; Nichols, R. J.; Hardwick, L. J., Mechanistic Insight into the superoxide induced ring opening in propylene carbonate based electrolytes using in situ surface-enhanced infrared spectroscopy. *J. Am. Chem. Soc.* **2016,** *138* (11), 3745-3751.
45. Hartstein, A.; Kirtley, J. R.; Tsang, J. C., Enhancement of the infrared-absorption from molecular monolayers with thin metal overlayers. *Phys. Rev. Lett.* **1980,** *45* (3), 201-204.
46. Hatta, A.; Ohshima, T.; Suetaka, W., Observation of the enhanced infrared-absorption of para-nitrobenzoate on ag island films with an atr technique. *Applied Physics a-Materials Science & Processing* **1982,** *29* (2), 71-75.
47. Kretschmann, E., *Z. Phys.* **1971,** *241*, 313-324.
48. Osawa, M.; Ikeda, M., Surface-enhanced infrared absorption of p-nitrobenzoic acid deposited on silver island films: contributions of electromagnetic and chemical mechanisms. *The Journal of Physical Chemistry* **1991,** *95* (24), 9914-9919.
49. Miyake, H.; Ye, S.; Osawa, M., Electroless deposition of gold thin films on silicon for surface-enhanced infrared spectroelectrochemistry. *Electrochemistry Communications* **2002,** *4* (12), 973-977.
50. Osawa, M., Surface-enhanced infrared absorption. *Near-Field Optics and Surface Plasmon Polaritons* **2001,** *81*, 163-187.
51. Osawa, M.; Ataka, K.; Yoshii, K.; Nishikawa, Y., Surface-enhanced infrared-spectroscopy - the origin of the absorption enhancement and band selection rule in the infrared-spectra of molecules adsorbed on fine metal particles. *Applied Spectroscopy* **1993,** *47* (9), 1497-1502.
52. Frisch, M.; Trucks, G.; Schlegel, H.; Scuseria, G.; Robb, M.; Cheeseman, J.; Scalmani, G.; Barone, V.; Mennucci, B.; Petersson, G., Gaussian 09, rev. A. 02. *Gaussian Inc., Wallingford, CT* **2009**.
53. Pople, J. A.; Headgordon, M.; Raghavachari, K., Quadratic configuration-interaction - a general technique for determining electron correlation energies. *J. Chem. Phys.* **1987,** *87* (10), 5968-5975.

54. Zhao, Y.; Truhlar, D. G., Density functionals with broad applicability in chemistry. *Accounts of Chemical Research* **2008,** *41* (2), 157-167.

55. Gao, X. W.; Chen, Y. H.; Johnson, L.; Bruce, P. G., Promoting solution phase discharge in Li-O_2 batteries containing weakly solvating electrolyte solutions. *Nature Materials* **2016,** *15* (8), 882-+.

56. Abate, II; Thompson, L. E.; Kim, H. C.; Aetukuri, N. B., Robust NaO_2 electrochemistry in aprotic Na-O_2 batteries employing ethereal electrolytes with a protic additive. *Journal of Physical Chemistry Letters* **2016,** *7* (12), 2164-2169.

57. Kwabi, D. G.; Batcho, T. P.; Feng, S. T.; Giordano, L.; Thompson, C. V.; Shao-Horn, Y., The effect of water on discharge product growth and chemistry in Li-O_2 batteries. *Physical Chemistry Chemical Physics* **2016,** *18* (36), 24944-24953.

58. Schwenke, K. U.; Metzger, M.; Restle, T.; Piana, M.; Gasteiger, H. A., The Influence of water and protons on Li_2O_2 crystal growth in aprotic Li-O_2 cells. *Journal of the Electrochemical Society* **2015,** *162* (4), A573-A584.

59. Wilmarth, W. K., Volnov,I. I., Peroxides superoxides and ozonides of alkali and alkaline earth metals. *American Scientist* **1967,** *55* (4), A468-&.

60. Zhu, Y. G.; Liu, Q.; Rong, Y.; Chen, H.; Yang, J.; Jia, C.; Yu, L.-J.; Karton, A.; Ren, Y.; Xu, X.; Adams, S.; Wang, Q., Proton enhanced dynamic battery chemistry for aprotic lithium–oxygen batteries. *Nature Communications* **2017,** *8*, 14308.

61. Das, U.; Lau, K. C.; Redfern, P. C.; Curtiss, L. A., Structure and stability of lithium superoxide clusters and relevance to Li–O_2 batteries. *The Journal of Physical Chemistry Letters* **2014,** *5* (5), 813-819.

62. Reinsberg, P.; Weiß, A.; Bawol, P. P.; Baltruschat, H., Electrochemical reaction order of the oxygen reduction reaction in Li^+-containing DMSO. *The Journal of Physical Chemistry C* **2017,** *121* (14), 7677-7688.

63. Mason, D.; Magdassi, S.; Sasson, Y., Interfacial activity of quaternary-salts as a guide to catalytic performance in phase-transfer catalysis. *Journal of Organic Chemistry* **1990,** *55* (9), 2714-2717.

64. Aldous, I. M.; Hardwick, L. J., Influence of tetraalkylammonium cation chain length on gold and glassy carbon electrode interfaces for alkali metal-oxygen batteries. *Journal of Physical Chemistry Letters* **2014,** *5* (21), 3924-3930.

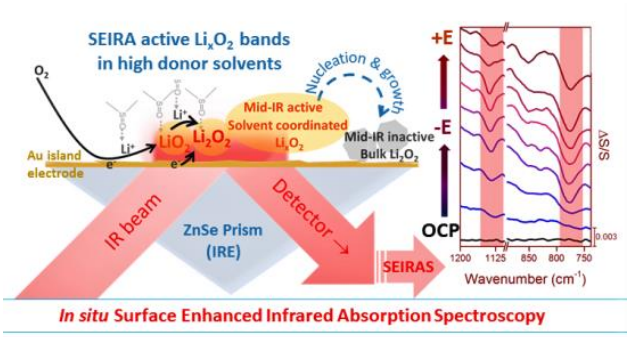
SEIRA active Li_xO_2 bands
in high donor solvents
Nucleation & Growth
Mid-IR active
Solvent coordinated
Li_xO_2
Mid-IR inactive
Bulk Li_2O_2
Au island
electrode
IR beam
ZnSe Prism
(IRE)
Detector
SEIRAS
+E
-E
OCP
ΔS/S
0.003
1200
1125
850
800
750
Wavenumber (cm^{-1})
In situ Surface Enhanced Infrared Absorption Spectroscopy

TOC Graphic